Eur. J. Mech. B/Fluids, **18**, n° 2, 173-196, 1999

Flow through and particle interception by an infinite array of closely-spaced circular cylinders

F. AYAZ [a], T.J. PEDLEY [b]*

ABSTRACT. – Steady two-dimensional laminar flow through an infinite array of parallel circular cylinders is computed numerically for values of the Reynolds number Re, based on oncoming velocity and cylinder diameter, up to 40, and for values of the spacing parameter, W (the ratio of the distance between cylinder axes to the cylinder radius), ranging from 2.3 to 10. The method used is that of Fornberg (1991). Results are presented for the dimensionless drag on a cylinder, D (or, equivalently, the dimensionless permeability of the array, $\beta = W/D$) and are compared with previous analytical results for very small Re and either wide or very narrow gaps. Results are also presented for the efficiency with which a filter consisting of such an array would capture spherical particles of radius b by direct interception, assuming that particle centres follow streamlines and that a particle is captured whenever it touches a cylinder. Such results are applicable to the study of filter feeding by small aquatic organisms. © Elsevier, Paris.

1. Introduction

The problem investigated in this paper was motivated by a research area of ecological importance, the feeding by filtration of small aquatic organisms. Suspension or filter feeding is widespread among planktonic and other aquatic animals of a variety of types: ciliated protozoa, crustacea, echinoderms, bivalve molluscs, fish, etc; see Jørgenson (1966) for a review. Such organisms use feathery or ciliary appendages held at an appropriate orientation to the ambient water flow or moved relative to the water, and the filter extracts food particles from the water.

Biological filters are commonly made up of cylindrical fibrous elements which are arranged in a roughly parallel or rectangular mesh, and may be internal or external to the organism. In most but not all cases the Reynolds number of an individual filter element is small, though the Reynolds number for the filter as a whole is often not small (Cheer and Koehl, 1987; Silvester, 1987). Examples include the filters on the maxillae or appendages of small crustacea, such as the calanoid copepod, *Eucalanus pileatus*, or the cladoceran, *Daphnia parvula*. Both the first maxilla of the former, and the third thoracic appendage of the latter, consist of a sparse array of relatively large parallel setae off which branches a more closely spaced array of finer setules (Cheer and Koehl, 1987). Dimensions are given in *table I*, as are typical values of the relative velocity of the filter and the water. It can be seen that the Reynolds number of a filter element (based on diameter — see eq (1.1) below) ranges from 5×10^{-5} (setules of *D. parvula*) to 0.1 (setae of *E. pileatus*). There are other organisms with larger filter spacing and larger Reynolds number, such as the cephalic fan rays of the larva of the black fly, *Similium vittatum*, whose dimensions are also listed in *table I*. Here the Reynolds number of the filter element can be as large as 4. In the crustacean examples, the length of the setules (about half the spacing of the setae) is much

* Correspondence and reprints.
[a] Matematik Ana Bilim Dali, Necatibey Egitim Fakulti, Balikesir University, Turkey.
[b] Department of Applied Mathematics & Theoretical Physics, University of Cambridge, UK.

0997-7546/99/02/© Elsevier, Paris

greater than their spacing; so to a first approximation the filter can be regarded as a two-dimensional array of parallel setules, rather than the actual array of long, narrow rectangles. The cephalic fan rays of the black fly larva can also be so modelled, although they are not precisely parallel.

TABLE I. – Dimensions and velocities of certain invertebrate filter elements.
The spacing is defined as the distance between the centres of neighbouring parallel filter elements. (Source: Cheer and Koehl, 1987.)

Species	Structure	Element	Diameter ($2a : \mu m$)	Spacing ($Wa : \mu m$)	Relative velocity ($U_0 : mms^{-1}$)
Daphnia parvula	3rd thoracic appendage	Seta Setule	1.8 0.32	6.8 0.68	0.15
Eucalanus pileatus	First maxilla	Seta Setule	7.0 2.0	31.0 6.0	15
Similium vittatum	Cephalic fan	Ray	5.0	35.0- 50.0	Up to 800

A food particle that is being carried along with the fluid that passes between the filter elements may be captured or may escape. In part this depends on the particle capture mechanism; a variety of different mechanisms exist, among them sieving, direct interception, inertial impaction, gravitational deposition, electrostatic deposition, Van der Waals attraction, etc (Rubenstein and Koehl, 1977). Although many of the above mechanisms are important for filter feeding, it has been shown that the sieving and the direct interception mechanisms are the most important for aquatic filter feeders capturing neutrally buoyant particles. Sieving occurs if the space between the filter elements is smaller than the width of the particle. A particle which is being carried along a streamline that crosses the filter cannot itself go through and must be captured whether the filter elements are sticky or not. Many filter feeders, such as caddisfly larvae, barnacles and protozoans, seem to retain a considerable number of food particles in this way. However, sieving cannot explain all of the observations which show that particles smaller than the filtering spaces are also captured (Jørgenson, 1983; LaBarbera, 1984). Capture by the direct interception mechanism assumes that at low particle Reynolds number the centre of a neutrally buoyant spherical particle follows an undisturbed streamline around a filtering fibre. If the streamline, and hence the centre of the particle, passes within one particle radius of the fibre surface, contact occurs and the particle is assumed to be retained by adhesion or electrostatic forces.

The assumption that food particles are effectively neutrally buoyant needs to be checked, since most of the microorganisms which would constitute the food have a density, ρ_p, around 5% greater than that of water, ρ (depending on the salinity). The Stokes number,

$$St = \frac{2}{9} b^2 \rho_p \frac{aU_0}{\mu}$$

measures the relative importance of inertial impaction to direct interception (Russel *et al.*, 1989); here a is the radius of the filter element, ba the radius of the particle, U_0 the relative velocity of fluid and filter element, and μ the fluid viscosity. For the crustacean filters listed in *table I* the Stokes number does not exceed 0.012 for $b = 1$; even for the black fly larva, St is only about 0.5 for $b = 1$. We therefore conclude that inertial impaction is not a major capture mechanism in the present context.

It might be thought that the best way to catch more small particles would be to decrease the spacing between filter elements. However, that is not necessarily true for an external filter because, as the permeability is decreased, more of the ambient flow passes round the edge of the filter, and the particles in it are not captured. Thus an optimum filter spacing will be predicted for a given size of food particle (Loudon and Alstad, 1990). Another reason to keep a high permeability is to prevent the pressure drop across the filter, $\Delta\hat{p}$, becoming so large as to damage the filter. Similarly for internal filters, $\Delta\hat{p}$ must remain low enough both to avoid damage and to keep down the energetic cost of pumping fluid through the filter; an optimum filter spacing is again anticipated.

In each case, the relevant fluid mechanical problem can be split into two parts: an inner problem, in which the pressure drop and particle capture properties of individual filter elements are computed, given a certain flow rate across unit area of filter; and an outer problem, in which the distribution of through flow and the total particle capture efficiency are obtained, given the overall relative velocity of fluid and filter, using the results of the inner problem.

This paper is concerned with the inner problem; subsequent papers will use the results in the outer problem and solve the overall optimisation problems mentioned above. We consider steady, two-dimensional, incompressible, viscous fluid flow through an infinite array of identical, equally-spaced circular cylinders of radius a and distance aW between their axes (see *figure 1* and *table I*); this is the simplest "inner problem" to solve precisely and is a good approximation in many cases. The fluid velocity far away is perpendicular to the plane of the array and has magnitude U_0. The Reynolds number is defined as

$$Re = 2aU_0/\nu \tag{1.1}$$

where $\nu = \mu/\rho$ is the kinematic viscosity of the fluid, μ and ρ being its dynamic viscosity and density. We shall seek numerical solutions to this problem for values of Re between 0 and 40, and for values of the spacing parameter W between 2.3 and 10 (note that the minimum gap width between two adjacent cylinders is $(W-2)a$). In addition to computing the streamline and vorticity patterns, the objectives of the study will be to compute the drag per unit length on an individual cylinder, $\mu U_0 D$, and the particle capture efficiency, $\eta(b)$, of the filter. Here ba is taken to be the radius of spherical neutrally buoyant particles being captured by direct interception, and η is defined as the number of particles per second captured by unit area of filter, divided by the number per second approaching unit area of the filter. Both D and η will depend on Re and W.

A momentum balance on a control volume extending far upstream and downstream, with its edges on planes of symmetry between cylinders, gives the pressure drop across the filter as

$$\Delta\hat{p} = \hat{p}(-\infty) - \hat{p}(+\infty) = \mu U_0 D/aW. \tag{1.2}$$

Thus the permeability of the filter, k, defined as flow rate per unit force, is given by

$$k = \frac{aWU_0}{\mu U_0 D} = \frac{U_0}{\Delta\hat{p}}. \tag{1.3}$$

This problem has been considered before, for different ranges of the parameters Re and W, by a number of authors. Tamada and Fujikawa (1957) gave an analytical solution for steady, two-dimensional, low Reynolds number flow through an infinite array of widely spaced circular cylinders ($W \gg 1, Re \ll 1$) on the basis of Oseen's equations, and calculated the dimensionless drag in the form

$$D = \frac{8\pi}{\Lambda}. \tag{1.4}$$

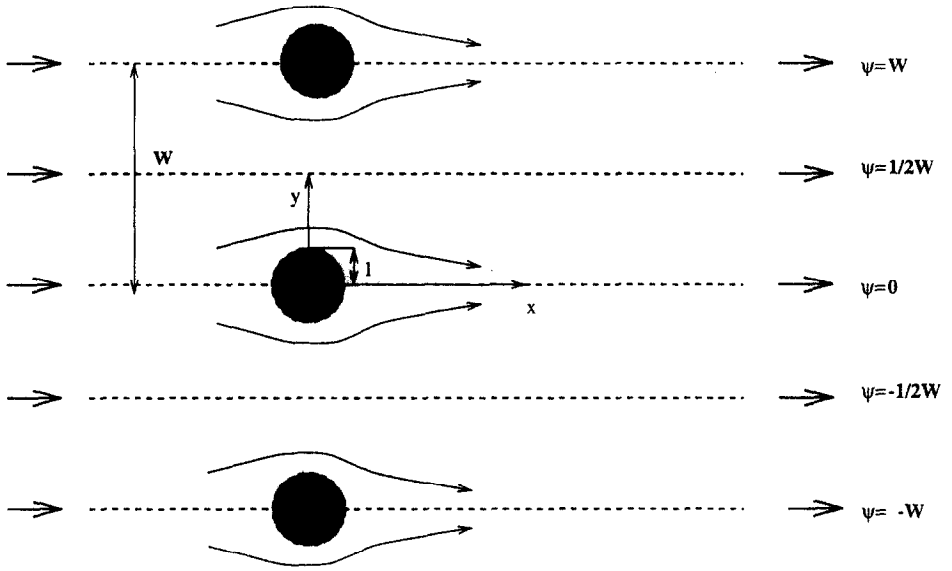

Fig. 1. – Flow configuration with dimensionless stream function values marked. Dotted lines show the planes of symmetry. W is the dimensionless distance between the centres of two cylinders, which have unit radius.

For $Re = 0, \Lambda$ was found to be

$$\Lambda = 1 - 2\log\tau + \frac{1}{6}\tau^2 - \frac{1}{144}\tau^4 + \frac{1}{1080}\tau^6 - \frac{53}{345600}\tau^8 + \frac{139}{5443200}\tau^{10} + 0(\tau^{12}), \tag{1.5}$$

where $\tau = 2\pi/W$. Another analytical treatment of the problem was given by Keller (1964). He investigated the problem of viscous flow through a closely packed lattice of circular cylinders ($W - 2 \ll 1, Re \ll 1$) using lubrication theory, and obtained a formula for the pressure drop as a function of the diameter-spacing ratio of the cylinders, $2/W$, which can be reduced to:

$$D = \frac{9\pi}{2W^{1/2}}(1 - 2/W)^{-5/2}. \tag{1.6a}$$

Keller himself quoted the expression

$$D = \frac{9\pi}{2^{3/2}}(1 - 2/W)^{-5/2}, \tag{1.6b}$$

having made use of the approximation $W \approx 2$.

The first numerical treatment of the problem for non-zero Re was given by Gordon (1978). His method was based on a uniform grid and a fourth-order accurate finite-difference scheme. He initially made calculations for $W = 6$ and then extended his work to a rectangular array of cylinders spaced in a finite number of infinite parallel rows. He plotted only the flow patterns for $Re = 1$ and $Re = 20$ and these results are consistent with the present predictions; the drag on the cylinders was not computed.

A study of Stokes flow ($Re = 0$) past rectangular as well as linear arrays of cylinders was made by Hildyard (1987) using the boundary-element method. For the linear array, such as ours, he computed the pressure drop

for values of W down to about 2.1, and showed increasingly good agreement with the lubrication theory result as $W - 2$ became smaller. He also computed the particle collection efficiency, but for very small particles whose density is much greater than that of the fluid so their trajectories were not the same as streamlines and directly intercepted the fibre elements. His results were compared with those of McLaughlin *et al.* (1986), who computed the same particle collection efficiency but at non-zero Reynolds number (and with questionable attention to accuracy).

The most relevant previous work is that of Fornberg (1991) whose interest was in high Reynolds number (≥ 100) and relatively large W. He used two numerical codes which he called the wide and narrow codes, respectively. The wide code was developed for $W \geq 40$ whereas for the narrow code, $5 \leq W \leq 40$. In this study, Fornberg used a numerical method which was quite similar to that of his previous work on flow past a single cylinder (Fornberg 1980, 1985,1988). Briefly, the technique is based on iteration by Newton's method; the two-dimensional steady Navier-Stokes equations are expressed as a single equation for the stream function and this is solved by a second-order finite-difference scheme on the conformally mapped and stretched plane. He also applied new downstream and far field boundary conditions and obtained accurate results for Reynolds numbers up to 800 (for the wide code).

Our study is based on Fornberg's (1991) narrow code but differs in that we are interested in much smaller gaps between the cylinders. Calculations have been made for $W = 10, 5, 3, 2.5$ and 2.3 (when $W = 2.3$, the gap width is 0.3) and Reynolds numbers $0 \leq Re \leq 40$. ($Re = 40$ was taken as the upper limit because flow past cylinders becomes unsteady and asymmetric at about that value, and in any case there is little biological relevance for higher values.)

Solutions have been obtained to the equations of steady, two-dimensional motion by a finite-difference approximation in the conformally mapped plane. We follow the method of Fornberg (1991), but use somewhat different far field boundary conditions, as specified below. The results for dimensionless drag D, or permeability k, are compared with previous results where possible. In all cases the particle capture efficiency is also computed for various values of the particle size b.

2. Dimensionless formulation of the problem and boundary conditions

The Navier-Stokes and continuity equations are rewritten in stream-function-vorticity ($\psi - \omega$) form and made dimensionless with length-scale a (the cylinder radius) and velocity scale U_0 (velocity at infinity). The resulting equations are

$$\frac{\partial^2 \psi}{\partial x^2} + \frac{\partial^2 \psi}{\partial y^2} + \omega = 0, \tag{2.1}$$

$$\frac{\partial^2 \omega}{\partial x^2} + \frac{\partial^2 \omega}{\partial y^2} + \frac{Re}{2}\left(\frac{\partial \psi}{\partial x}\frac{\partial \omega}{\partial y} - \frac{\partial \psi}{\partial y}\frac{\partial \omega}{\partial x}\right) = 0, \tag{2.2}$$

where the dimensionless velocity components (u, v) in the (x, y) directions are given by

$$u = \frac{\partial \psi}{\partial y}, v = -\frac{\partial \psi}{\partial x}. \tag{2.3}$$

The dimensionless coordinate system is shown in *figure 1*. The flow is assumed to be symmetric about the x-axis and about the planes $y = \pm W/2$ etc., so the computational domain in the physical plane is the strip $0 \leq y \leq W/2$ with the semicircle $r = (x^2 + y^2)^{1/2} \leq 1$ taken out. The boundary conditions are

$$\psi = \frac{\partial \psi}{\partial r} = 0 \quad \text{on the body surface } r = 1 \quad \text{(no slip)}, \tag{2.4a}$$

$$\psi = \omega = 0 \quad \text{on} \quad y = 0, \quad |x| > 1, \tag{2.4b}$$

$$\psi = \frac{1}{2}W, \quad \omega = 0 \quad \text{on} \quad y = \frac{1}{2}W, \ -\infty < x < \infty, \tag{2.4c}$$

$$\psi \to y \quad \text{and} \quad \omega \to 0 \text{ as } x \to \pm\infty, 0 \le y \le \frac{1}{2}W. \tag{2.4d}$$

The implementation of the boundary conditions at large distances will be discussed in the following sections.

The drag on one cylinder is obtained by integrating the x-component of stress over the body surface $r = 1$, and is given in terms of polar coordinates (r, θ) by

$$D = 2\int_0^{\pi} \left(\frac{\partial \omega}{\partial r} - \omega\right) \sin\theta d\theta, \tag{2.5}$$

evaluated at $r = 1$.

3. Computational domain

Following Fornberg (1991) we transform the physical domain into a parallel-sided strip, using a conformal mapping to take the physical complex plane, $X = x + iy$, to the computational complex plane, $Z = \xi + i\eta$, (see *figure 2*). The analytical expression for the mapping is given by Fornberg as follows:

$$Z = \frac{V}{W}\{X + \alpha_1 T + \alpha_2 T^3 + \alpha_3 T^5 + \cdots\}, \tag{3.1}$$

where the real coefficients V and $\{\alpha_i\}, i = 1, 2, \ldots$, have to be evaluated, $\frac{W}{2}, \frac{V}{2}$ indicate the widths of the physical and the computational strips, respectively, and T is given by the relation

$$T = \frac{\pi}{W}\coth\left(\frac{\pi}{W}X\right). \tag{3.2}$$

By this transformation $0 \le y \le \frac{1}{2}W$ maps to $0 \le \eta \le \frac{1}{2}V$ and the coefficients must be evaluated so that the unit semi-circle maps to the segment $-2 \le \xi \le 2$ of the $\eta = 0$ axis. For any real values of the parameters V and α_i, equations (3.1) and (3.2) give

$$y = 0 \to \eta = 0$$
$$y = \frac{1}{2}W \to \eta = \frac{1}{2}V.$$
$$-1 \le x \le 1, \quad y = 0 \to -2 \le \xi \le 2, \ \eta = 0.$$

The transformed governing equations (2.1), (2.2) are unchanged, apart from the Jacobian factor $|dZ/dX|^2$ multiplying the Laplacian of ψ in (2.1). The expression (2.5) for the dimensionless drag, D, can be evaluated from the solution in the Z-plane by noting that, because the transformation is conformal, we can put $\sin\theta = y(\xi)$ and

$$r d\theta = \frac{1}{|dZ/dX|} d\xi$$

on the cylinder surface. Then (2.5) becomes

$$D = 2\int_{-2}^{2} \left(\frac{\partial \omega}{\partial \eta} - \frac{\omega}{|dZ/dX|}\right) y(\xi) d\xi. \tag{3.3}$$

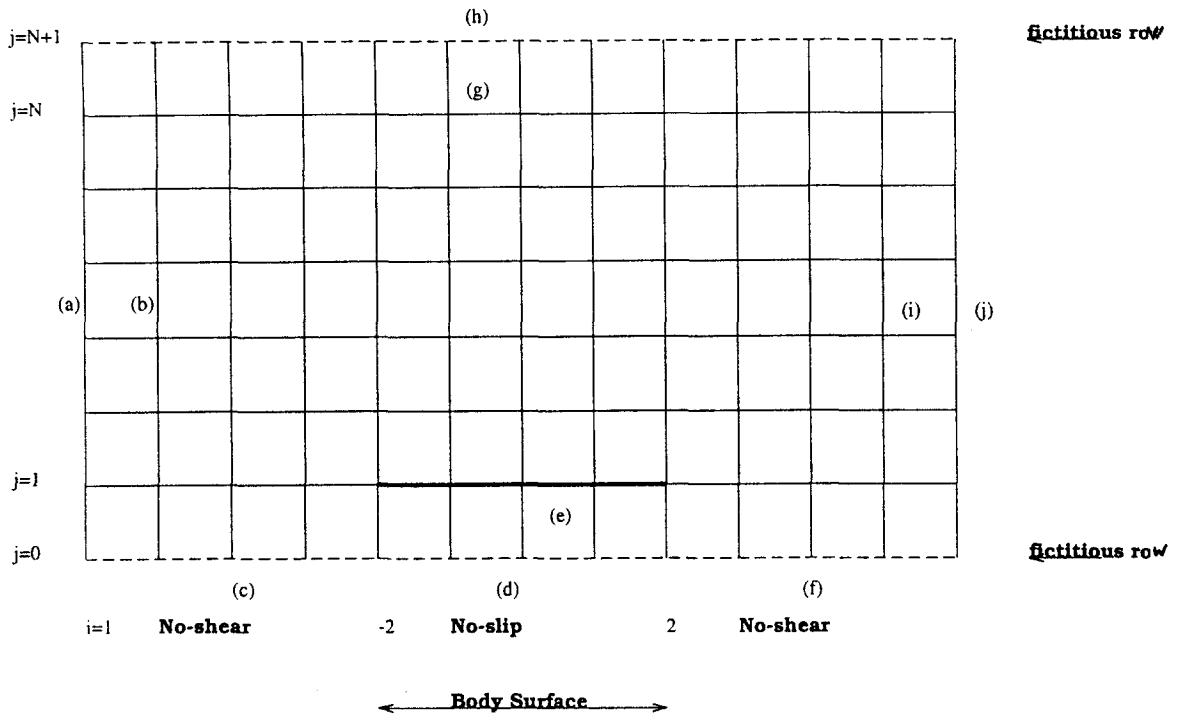

Fig. 2. – Computational plane. Letters (a)-(j) show the rows and columns at which boundary conditions (a-j) are applied. Two fictitious rows are added in order to apply the conditions (a,b,i,j).

It proves to be additionally convenient, in the computations, to let the stream function vary between 0 and 1 instead of 0 and $\frac{W}{2}$, so both ψ and ω are multiplied by $2/W$, and Re in (2.2) is replaced by $Re' = \frac{W}{2}Re$.

For each value of W, the coefficients $\{\alpha_i\}$ and V are evaluated by using the Laurent expansion of the right hand side of (3.1), and requiring that its imaginary part be zero when $|X| = 1(y \geq 0)$, and that $Z = 2$ when $X = 1$ (see Fornberg, 1991). It turns out that the magnitude of α_i decreases rapidly as i increases, especially for larger values of W; for each W, all α_i with magnitudes in excess of 10^{-8} were computed. The computed values of V and $\{\alpha_i\}$, for various values of W, are given in *table II*. The values for $W = 10$ and $W = 5$ are the same as those given by Fornberg (1991).

In order to set up the finite-difference versions of the governing equations, the Z plane is discretised into a uniform grid with mesh spacings h, k (not necessarily equal) along the ξ and η axes, respectively. The upstream and downstream boundary locations, $\xi = \xi_u$ and $\xi = \xi_d$ respectively, can be chosen arbitrarily, subject to being far enough away that the choice does not influence the results.

For every grid point (ξ, η) in the Z plane, it is necessary to determine the corresponding point (x, y) in the physical, X, plane. For a given W, the computed values of $\{\alpha_i\}, V$ are substituted into (3.1) which becomes a nonlinear equation in the two variables (x, y). This is solved for each (ξ, η) using the well-known method of Powell (1970).

4. Numerical method

Discretisation

Following Fornberg (1991), we discretise the transformed governing equations using second-order-accurate, central finite differences. The computational domain (*figure 2*) is overlaid by a uniform rectangular grid; the

TABLE II. – The coefficients V and α_i for different cylinder spacings W.

	W = 10	W = 5	W = 3	W = 2.5	W = 2.3
V	9.67308621	4.35640639	1.94496482	1.22143989	0.88410558
α_1	1.03404008	1.15317637	1.63356885	2.41214590	3.47585250
α_2	-0.00022418	-0.00409426	-0.05340594	-0.21376459	-0.57020762
α_3	0.00000211	0.00015599	0.00639234	0.04692995	0.19814748
α_4	-0.00000002	-0.00000624	-0.00081183	-0.01135289	-0.07873897
α_5		0.00000025	0.00010579	0.00292280	0.03396165
α_6		-0.00000001	-0.00001406	-0.00079015	-0.01546069
α_7			0.00000190	0.00022190	0.00729529
α_8			-0.00000026	-0.00006415	-0.00352758
α_9			0.00000004	0.00001894	0.00173545
α_{10}				-0.00000567	-0.00086407
α_{11}				0.00000171	0.00043289
α_{12}				-0.00000052	-0.00021627
α_{13}				0.00000015	0.00010619
α_{14}				-0.00000004	-0.00005020
α_{15}				0.00000001	0.00002229
α_{16}					-0.00000906
α_{17}					0.00000328
α_{18}					-0.00000103
α_{19}					0.00000027
α_{20}					-0.00000006
α_{21}					0.00000001

vertical lines (ξ = const.) are labelled $i = 1$ to M, left to right, and the horizontal lines (η = const.) are labelled $j = 1$ to N, bottom to top. The vorticity is eliminated from the equations, to leave a single equation at each internal point (i, j), of the form

$$f_{i,j}(\psi_{i-2,j}, \ldots, \psi_{i+2,j}) = 0, \tag{4.1}$$

linking the values of ψ at 13 neighbouring points. The details of the discretisation are cumbersome and will not be given here (they can be obtained from the authors on request).

Boundary conditions

In order to use (4.1) at points close to the boundaries $\eta = 0, V/2$, two fictitious rows $j = 0$ and $j = N + 1$ are added to the computational grid. The standard boundary conditions on all parts of the domain boundary (lines (a)–(j), *figure 2*) are given in equations (4.2a–j) below. Wherever the boundary conditions refer to $\omega_{i,j}$, a central-difference representation of the transformed (2.1) is implied.

$$\psi_{1,j} = \eta_{1,j}/(V * 0.5) \text{ and } \omega_{1,j} = 0, \tag{4.2a}$$

$$\psi_{2,j} = \eta_{2,j}/(V * 0.5) \text{ and } \omega_{2,j} = 0, \tag{4.2b}$$

$$\psi_{i,0} = -\psi_{i,2}, \psi_{i,1} = 0, \text{ and } \omega_{i,1} = 0, \tag{4.2c}$$

$$\psi_{i,0} = \psi_{i,2}, \tag{4.2d}$$

$$\psi_{i,1} = 0 \text{ and } \omega_{i,1} \neq 0, \tag{4.2e}$$

$$\psi_{i,0} = -\psi_{i,2}, \ \psi_{i,1} = 0 \text{ and } \omega_{i,1} = 0, \tag{4.2f}$$

$$\psi_{i,N} = 1 \text{ and } \omega_{i,N} = 0, \tag{4.2g}$$

$$\psi_{i,N+1} = 2 - \psi_{i,N-1}, \tag{4.2h}$$

$$\frac{\partial \omega_{M-1,j}}{\partial \xi} = 0, \tag{4.2i}$$

$$\frac{\partial^2 \psi_{M,j}}{\partial \xi^2} = 0. \tag{4.2j}$$

In the above (4.2a,b) are boundary conditions upstream where the flow is the known uniform velocity. Eqs. (4.2i,j) give the downstream boundary conditions as prescribed by Fornberg (1991). He used the condition $\frac{\partial \omega}{\partial \xi} = 0$, which is implemented over two adjacent columns, to eliminate mesh-size oscillations which may arise from the use of the central finite-difference approximations to the derivatives in the equations. The discretisations of (4.2i,j) can also be obtained from the authors. In (4.2d and e), the no-slip boundary condition is applied on the cylinder surface; over the rest of the domain boundary, (4.2c,f,g,h) no-shear boundary conditions are applied.

Alternative, asymptotic, forms of the up- and downstream boundary conditions are also used (as in Ingham, Tao and Morton (1990)), both as a check on the accuracy of our results, especially for $Re > 6$, and in an attempt to reduce the size of the computational domain. These are described in the following subsection.

Asymptotic boundary conditions

A simple asymptotic solution to the equations (2.1) and (2.2), with Re' for Re, can be obtained for large negative and positive values of x, by writing

$$\psi = \frac{2}{W} y + f(y) e^{-\beta x}$$

and

$$\omega = g(y) e^{-\beta x}.$$

Upon substituting these expressions into the equations, and linearising, one can obtain solutions for the eigenvalue β and the eigenfunctions f, g as follows:

$$\beta_{+}^{-} = \frac{1}{2}\left[-\frac{Re'}{W} \mp \sqrt{\left(\frac{Re'}{W}\right)^2 + \left(\frac{2\pi}{W}\right)^2}\right] \quad \text{for } x \underset{>}{<} 0, \tag{4.3}$$

$$f(y) = A_n \sin\left(\frac{\pi}{W}y\right), g(y) = B_n \sin\left(\frac{\pi}{W}y\right),$$

with A_n, B_n real constants. Thus the asymptotic boundary conditions are

$$\frac{\partial\psi}{\partial x} = -\beta_-\left(\psi - \frac{2}{W}y\right), \quad \frac{\partial\omega}{\partial x} = -\beta_-\omega, \quad \text{as } x \to -\infty, \tag{4.4a}$$

$$\frac{\partial\psi}{\partial x} = -\beta_+\left(\psi - \frac{2}{W}y\right), \quad \frac{\partial\omega}{\partial x} = -\beta_+\omega, \quad \text{as } x \to \infty. \tag{4.4b}$$

After transformation, these conditions replace Eqs. 4.2a, b, i, j: their discretised forms can be obtained from the authors. Note that the ends of the domain are taken far enough away for $|\frac{dZ}{d\Lambda}| \sim 1$ so we may ignore this term in imposing the conditions. Moreover it is really only for larger values of Re', and downstream, that the value of β ($\beta+$) is not large enough for the perturbation to the uniform stream to die away rapidly, so it is only in such cases that the asymptotic boundary condition is essential.

Newton's Method

Since the finite-difference equations obtained from Eq. (4.1) are nonlinear, they are linearised and Newton's Method employed to solve them. The big advantage of Newton's Method is that it is quadratically convergent. The main disadvantages are that it uses a very large amount of computer memory, is computationally expensive, and requires that the initial guess at the solution is sufficiently close to the actual solution. For each value of W, the initial guess at the solution at $Re = 0$ is taken to be $\psi = \frac{2}{V}\eta$, the result for potential flow. The value of Re is then increased incrementally, the initial guess at each step being the solution for the previous value of Re.

The discretised form of (4.1) represents $(N-2)\times(M-2)$ or $(N-2)\times M$ equations (depending on which boundary conditions are used) for the $(N-2)\times(M-2)$ or $(N-2)\times M$ unknowns $(\psi_{11}, \ldots \psi_{1(N-2)}, \psi_{M(N-2)})$. From eq. (4.1) the unknown function ψ has to be evaluated at the nodes in the Z plane, ordered by columns, left to right; the coefficient matrix has banded structure, each minor submatrix is of size $(N-2)\times(N-2)$ and the system has M block rows when asymptotic boundary conditions are applied, or otherwise $M-2$ block rows. The matrix has band width $4\times N-7$, and contains $(M-2)\times(N-2)$ equations ($M\times(N-2)$ equations for asymptotic boundary conditions). The approximate solution of the set of linear banded equations has been obtained by the standard direct method of LU decomposition with partial pivoting. The details of the method can be found in Fox (1964), Wilkinson (1965), Wilkinson and Reinsch (1971) and Bohte (1975). Convergence occurs very rapidly near to the solution and the number of correct decimal places can be doubled in one iteration. For each case, three to five iterations were required to obtain converged solutions with residuals $< \epsilon = 10^{-6}$ (a few cases were tested with $\epsilon = 10^{-8}$, but no differences were found to 5 significant figures).

At each Newton iteration, the solution of the matrix equation involves approximately $16MN^3$ arithmetic operations. The choice of M and N, and the grid refinement tests undertaken, are described in the next section; the maximum number of node points used was $24932(271\times 92)$. The computations were carried out on the VPX 240/10 machine at the Manchester Computer Centre. A single Newton iteration took a maximum of 2 seconds; the memory requirement was 75MB.

5. Numerical results

5.1. Results for $W = 10$

The main aim of this computation is to obtain a numerical solution of the Navier-Stokes equations for the given geometry with $W \leq 5$ and values of the Reynolds number Re (not Re') up to 40. However, we begin by considering $W = 10$ because we wish to compare our computed drag values with the analytical results of Tamada and Fujikawa (1957) for this gap size and for Reynolds numbers up to 8. They also found a formula for $W = 5$, but the drag was given only for $Re = 0$.

Most of the numerical calculations were made in the computational domain $-7 \leq \xi \leq 7$, which corresponds to $-6.9 \lesssim x \lesssim 6.9$ in the physical plane, with $M = 211, N = 92$ (grid C). For accuracy checks, various different values of M and N were tried, as well as different downstream lengths and end boundary conditions, as specified in *table III*. The results for the dimensionless drag, D, calculated from the discretised form of (3.3), are given for the various grids in *table IV*. We can see that, at low Reynolds numbers, the grids with longer downstream length ξ_d (D and E) give excellent agreement with the analytic solution; grid C (a finer grid but with $\xi_d = 7$) also gives acceptable accuracy (see also *table VI* below, for $W = 5$). At larger Re (up to 8.0), the asymptotic boundary conditions (grids D', E') make only a small difference. To provide a further accuracy test, we also plot the wall vorticity on the cylinder (typically the most sensitive variable in fluid dynamic computations) for grids B and C. *Figure 3* shows this comparison for $Re = 10$ and $W = 10$. The small discrepancy between the finer and the coarser mesh indicates that the finer mesh (C) is accurate enough for numerical calculations. All calculations for $W < 10$, therefore, were performed using Grid C only. Some of the following results for $W = 10$ were obtained using grid E, because the additional downstream length is desirable for plotting streamlines or vorticity contours. However, as we shall see, the length of the physical domain corresponding to $-7 \leq \xi \leq 7$ increases as W is decreased, so grid C is good enough even for streamline plots.

Table III. – The computational grids used for grid refinement studies.
Grids A', D', E' are the same as grids A, D, E but use the asymptotic boundary conditions (4.4).

$W = 10$	ξ	h	k	M	N
Grid A	$-7 \leq \xi \leq 7$	1/10	0.5*V/45	141	46
Grid A' (asy.)	$-7 \leq \xi \leq 7$	1/10	0.5*V/45	141	46
Grid B	$-7 \leq \xi \leq 7$	1/10	0.5*V/61	141	62
Grid C	$-7 \leq \xi \leq 7$	1/15	0.5*V/91	211	92
Grid D	$-7 \leq \xi \leq 15$	1/10	0.5*V/91	221	92
Grid E	$-7 \leq \xi \leq 20$	1/10	0.5*V/91	271	92
Grid D' (asy.)	$-7 \leq \xi \leq 15$	1/10	0.5*V/91	221	92
Grid E' (asy.)	$-7 \leq \xi \leq 20$	1/10	0.5*V/91	271	92

Streamlines

From the numerical results using grid E, contours of ψ have been plotted to give the pattern of streamlines. *Figure 4* shows streamlines for $Re = 0, 5, 8, 10$ and 40 and $W = 10$. The patterns have similar features to

TABLE IV. – Comparison of dimensionless drag D computed using the different grids, together with that from the analytical solution of Tamada and Fujikawa (1957), for $W = 10$ and $0 \leq Re \leq 8$.

	Dimensionless Drag								
Re	Anal. Res.	*Grid A*	*Grid A'*	*Grid B*	*Grid C*	*Grid D*	*Grid E*	*Grid D'*	*Grid E'*
0.00	12.58	12.34	12.26	12.46	12.51	12.587	12.587	-	-
0.08	12.59	12.34	12.27	12.46	12.51	12.589	12.589	-	-
0.24	12.60	12.36	12.28	12.48	12.53	12.605	12.605	-	-
0.40	12.66	12.40	12.32	12.51	12.56	12.638	12.638	-	-
0.80	12.87	12.54	12.47	12.66	12.72	12.800	12.800	-	-
1.60	13.73	13.08	13.01	13.21	13.26	13.345	13.345	-	-
2.40	15.05	13.80	13.72	13.94	14.00	14.086	14.086	-	-
3.20	16.22	-	14.52	14.76	14.82	14.901	14.901	-	-
4.00	17.29	-	15.33	15.60	15.66	15.754	15.754	-	-
4.80	18.59	-	-	-	16.48				
5.60	19.85	-	-	-	17.32				
6.40	21.05	-	-	-	18.12	18.214	18.214	18.080	18.080
7.20	22.21	-	-	-	18.89	18.994	18.994	18.855	18.855
8.00	23.20	-	-	19.54	19.65	19.755	19.755	19.611	19.611

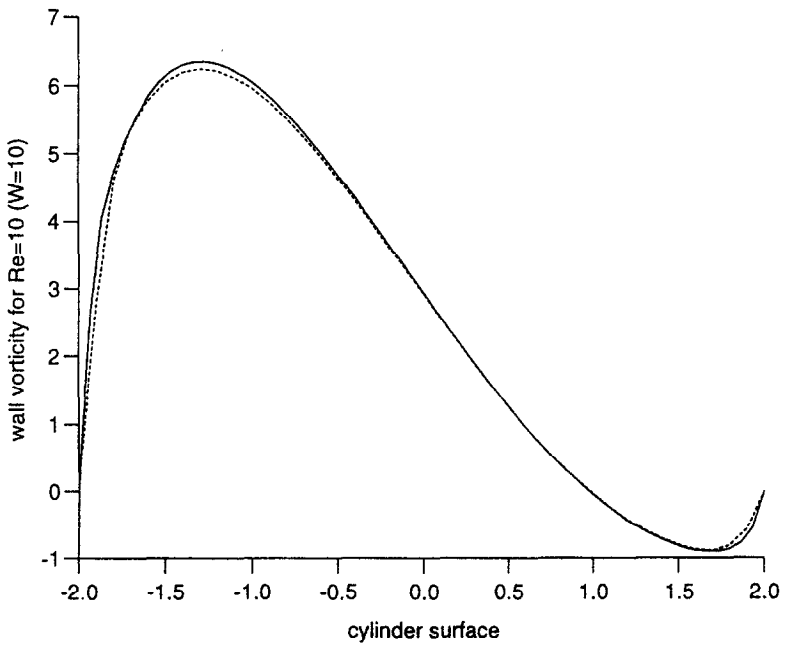

Fig. 3. – Comparison of wall vorticity as computed on the fine (*Grid C*) and coarse (*Grid B*) meshes; $Re = 10$, $W = 10$.

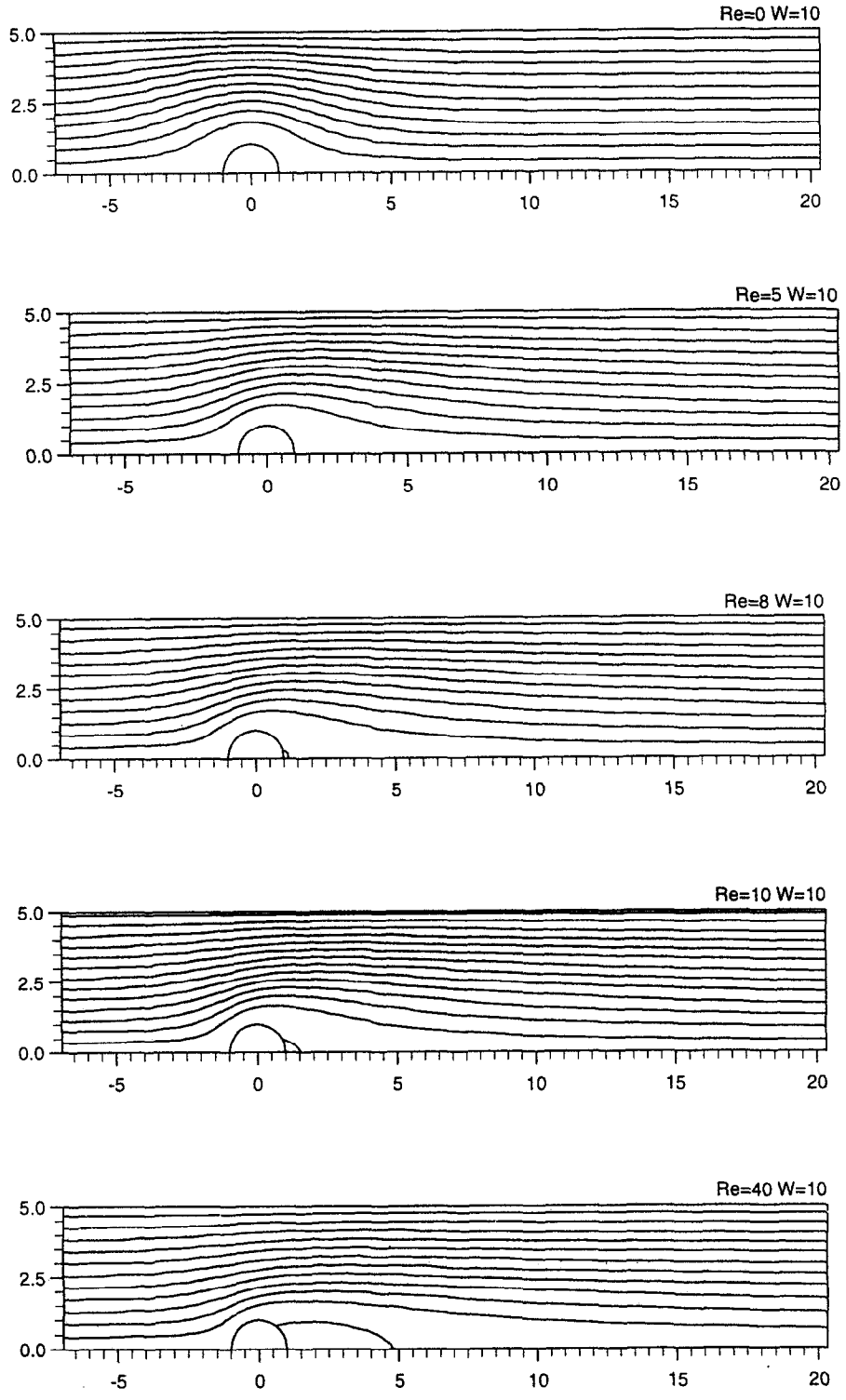

Fig. 4. – Streamlines with $\psi = 0, 0.1, 0.2 \ldots 1.0$ for $W = 10$ and $Re = 0, 5, 8, 10, 40$.

those shown for the flow past a single cylinder at comparable Reynolds numbers (Keller and Takami (1966), Fornberg (1985)). At zero Reynolds number there is Stokes flow which has fore and aft symmetry about the y axis. As the Reynolds number increases the flow becomes asymmetrical about this axis and for $Re \geq 8$ the boundary layers separate to form two symmetrical recirculation eddies.

Drag

Table IV gives the analytical and computed drag results for Reynolds number up to 8. The analytical results are obtained from (1.4) and (1.5) (Tamada and Fujikawa, 1957). As stated above, there is excellent agreement (for Grids C, D, E) at $Re = 0$. On increasing the Reynolds number considerable differences can be seen, but this is because the results of Tamada and Fujikawa (1957) are strictly valid only for $Re \ll 1$. They used the Oseen approximation for the problem, so inertia was taken into account, but the accuracy of their solutions must decline as Re increases.

TABLE V. – Computed dimensionless drag D for $0 \leq Re \leq 40$ and $W = 5.3.2.5.2.3.$

	Dimensionless Drag			
Re	W = 5	W = 3	W = 2.5	W = 2.3
0.00	31.70	153.41	559.33	1632.1
0.50	31.73	153.45	559.39	1632.2
0.80	31.80	153.51	559.48	1632.3
1.00	31.85	153.57	559.57	1632.5
2.40	32.60	154.35	560.75	1634.2
3.00	33.07	154.88	561.56	1635.6
3.20	33.25	155.08	561.88	1636.1
4.00	34.03	156.02	563.33	1638.4
5.00	35.16	157.48	565.63	1642.1
6.40	36.39	160.07	569.79	1648.8
7.20	37.97	161.81	572.68	1653.3
8.00	39.06	163.75	575.95	1658.7
10.00	41.84	169.35	585.84	1674.9
40.00	80.15	293.92	910.16	2353.0

5.2. RESULTS FOR $W \leq 5$

We now present results for the parameter range of greatest interest (to us): $W = 5, 3, 2.5$ and 2.3 and Re up to 40. By the transformation (3.1) the length of the physical domain increases with decreasing W in both negative and positive x directions. For example, the $-7 \leq \xi \leq 7$ interval in the computational plane corresponds to $-7.3 \lesssim x \lesssim 7.3$ for $W = 5, -9.14 \lesssim x \lesssim 9.14$ for $W = 3$ and $-13.14 \lesssim x \lesssim 13.14$ for $W = 2.3$; as stated above, *Grid C* has been used throughout. As we shall see, even the more sensitive drag results are not affected by the choice of boundary location.

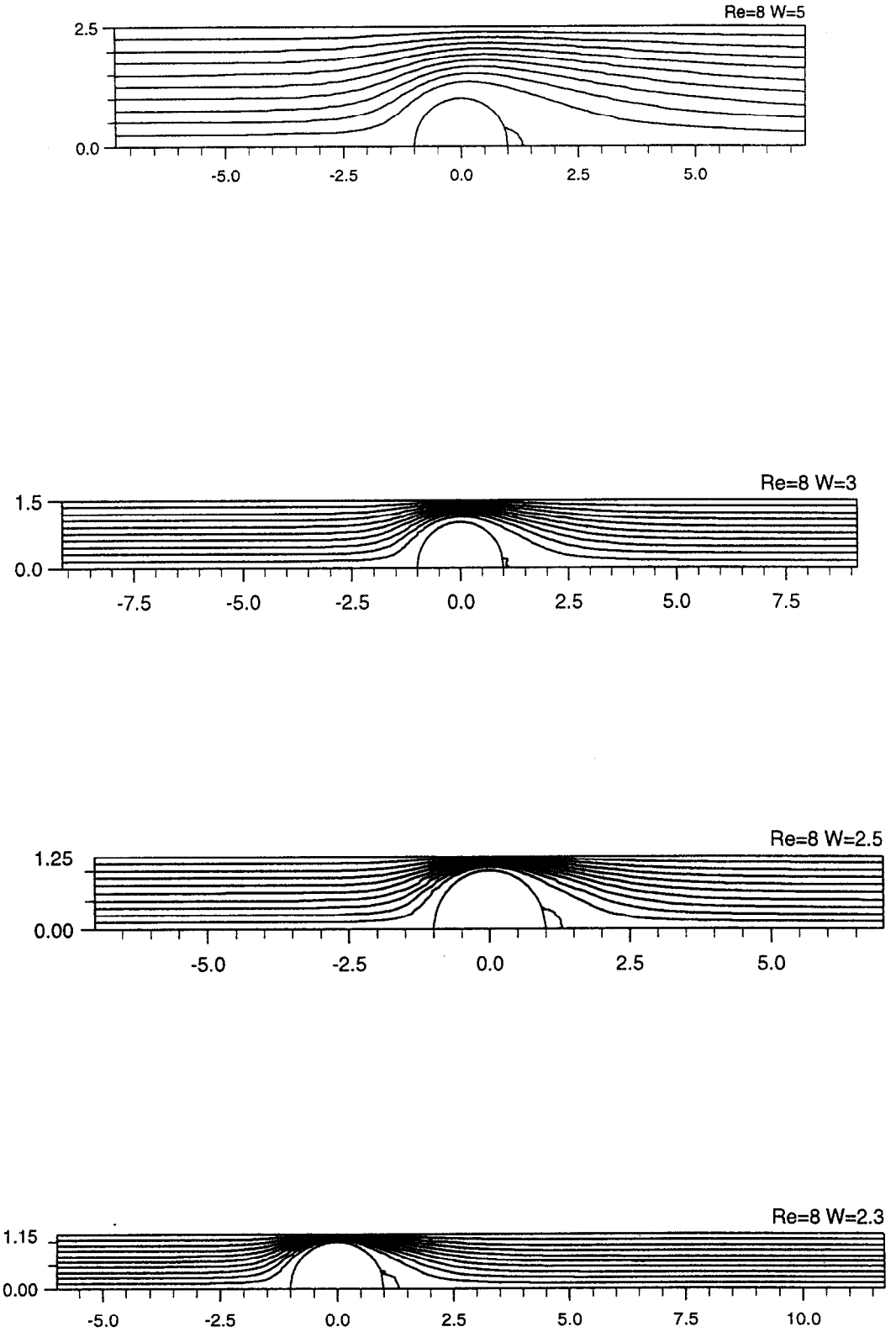

Fig. 5. – Streamlines, with spacing 0.1, for $Re = 8$ and $W = 5, 3, 2.5, 2.3$.

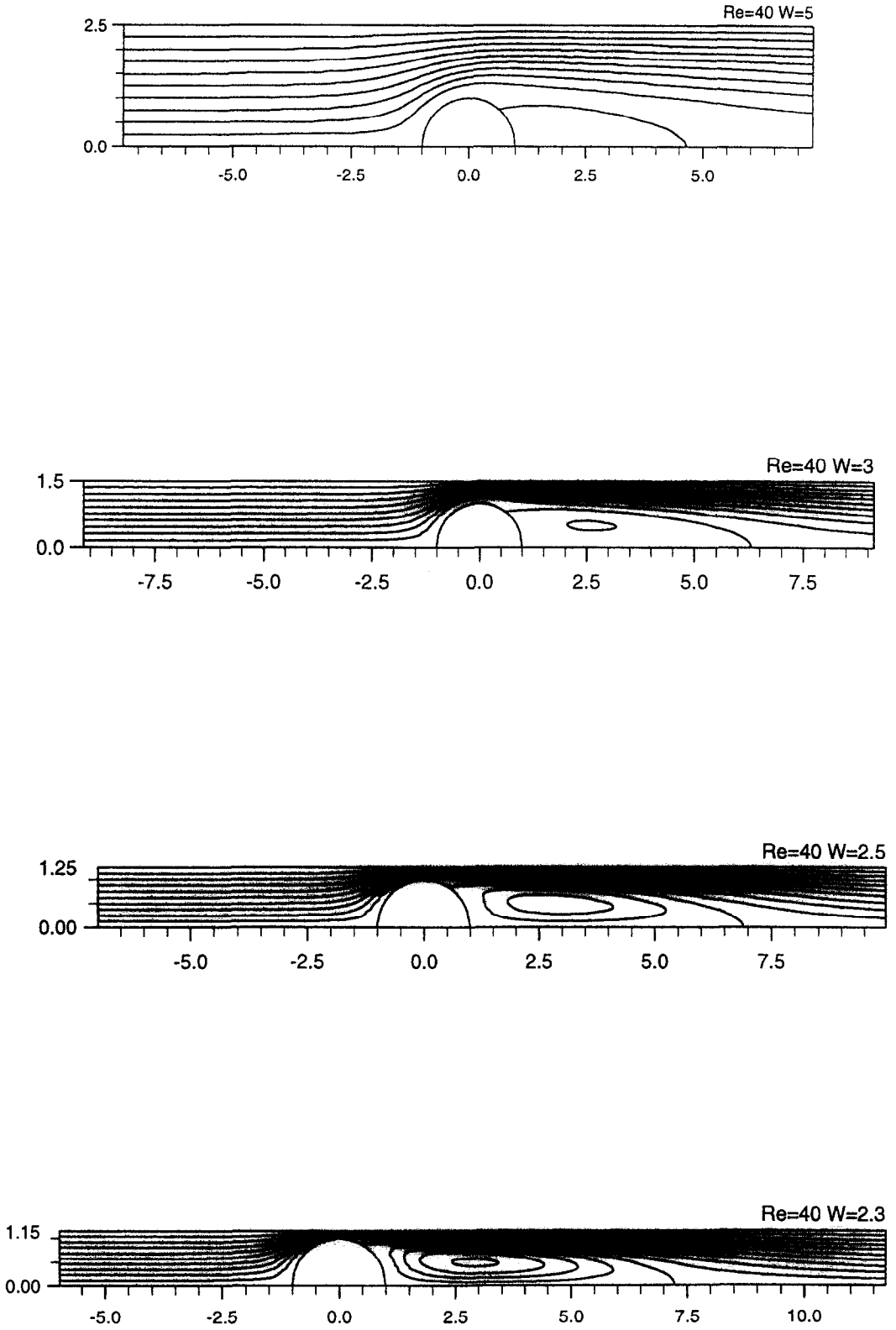

Fig. 6. – Streamlines, with spacing 0.1, for $Re = 40$ and $W = 5, 3, 2.5, 2.3$.

Streamlines and vorticity contours

There are no great surprises in the flow patterns, so we show only a selection of the computed results. Streamlines are shown in *figures 5* and *6* for $Re = 8$ and 40, respectively, for the range of different values of W. At $Re = 40$ the increasing strength of the separated flow eddy as W decreases can be clearly seen.

Solution of Eq. (4.1) does not involve the direct evaluation of the vorticity. After calculating the stream function ψ over the whole grid these values are substituted into the discretised version of (2.1) and the vorticity is computed at each point of the grid. At zero Reynolds number the vorticity contours are symmetrical about $y = 0$ and confined to a region near the cylinders whose length is comparable to the channel width. As the Reynolds number increases, the contours spread much further downstream because advection dominates viscous diffusion.

Figure 7 shows some of the vorticity contours; the vorticity and its gradient naturally become very large as the flow is squeezed between the cylinders at the smaller values of W. Greater detail in the streamline and vorticity plots for $W = 5, Re = 40$ are given in *figure 8*. The stronger jet and larger magnitude of vorticity at smaller W mean that appreciable vorticity extends somewhat further downstream, despite the fact that the decay rate $\beta+$ (eq. 4.3) is larger.

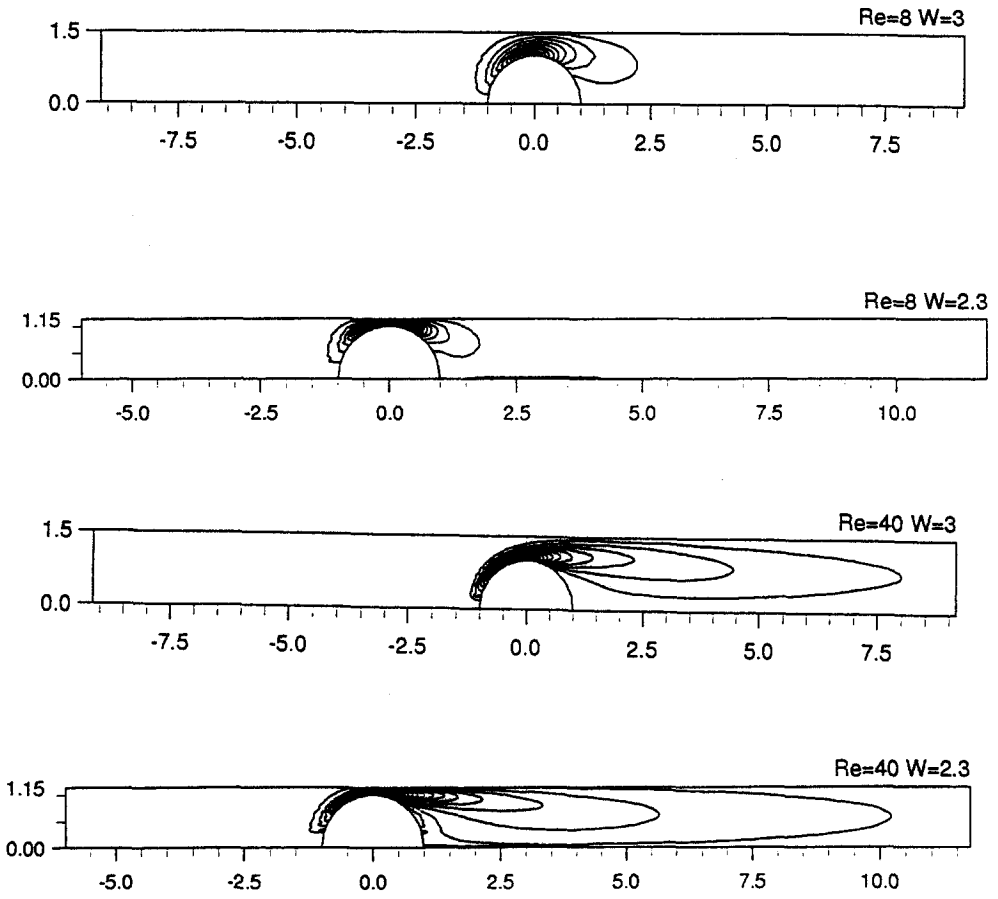

Fig. 7. – Vorticity contours for $Re = 8, 40$ and $W = 3, 2.3$.

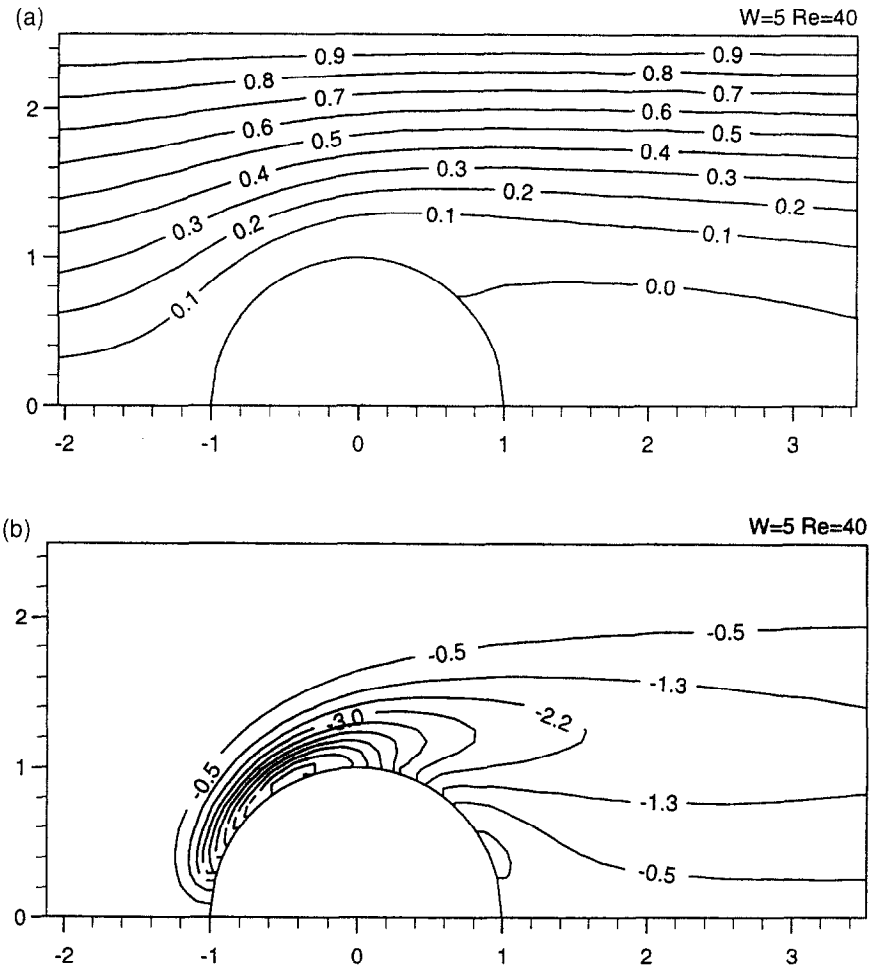

Fig. 8. – (a) Streamlines and (b) vorticity contours in the vicinity of the cylinder for $Re = 40, W = 5$.

The length of the recirculation region, defined as the difference between the x-values at the beginning and end of the dividing streamline, grows approximately linearly with Re, except at the smallest value of W. This can be seen in *figure 9*, where it is striking that the length grows more rapidly with Re for smaller gap width.

Drag

The drag on one of the cylinders in the array is obtained from equation (3.3) for $W = 5, 3, 2.5$ and 2.3 and $0 \leq Re \leq 40$; the results are shown in *table V*. It can be seen how dramatically the drag rises as W is reduced.

It would be desirable to test these computations by further comparisons with analytical solutions at zero Reynolds number. However, Tamada and Fujikawa's (1957) result (eqs. 1.4 and 1.5) is certainly not accurate for $W < 5$, while Keller's (1964) lubrication theory result (1.6a or b) is expected to be valid only for the smallest values of W. *Table VI* shows the computed drag results at zero Re and various values of W, as in the top row of *table V*, but now compared with the values obtained from equations (1.6a and b) and, at $W = 5$, from equations (1.4) and (1.5). It can be seen that, at $W = 5$, there is extremely good agreement with the wide gap formula of Tamada and Fujikawa (1957), while at lower values of W there is also excellent agreement with Keller's formula (1.6b), the error being only 1.6% for W as large as 3 (minimum gap width

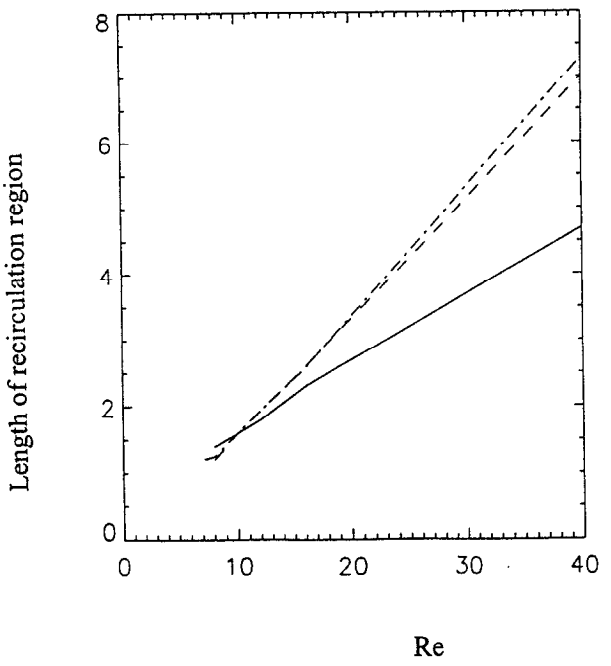

Fig. 9. – Length of recirculation region plotted against Re for $W = 5$ (solid curve), 2.5 (dashed curve), 2.3 (dash-dot curve).

TABLE VI. – Comparison of the drag results at $Re = 0$ with theoretical predictions, for $W = 5, 3, 2.5, 2.3$.

	Dimensionless Drag			
W	5	3	2.5	2.3
Computed drag values	31.69	153.4	559.3	1632
Keller's formula (1.6b)	35.85	155.8	558.8	1626
Formula (1.6a)	22.67	127.2	499.8	1517
Tamada & Fujikawa (1.4 and 1.5)	31.71	-	-	-

= one cylinder radius). This is remarkable. Even more remarkable is the fact that the excellent agreement is with equation (1.6b) rather than the apparently more appropriate (1.6a), which still differs from the computed values by 7% at $W = 2.3$. It should be noted that Keller's formula has previously been found to agree well with experiment: his prediction of $D = 2429$ from (1.6b) (or 2290 from (1.6a)) at $W = 2.25$ can be compared with a value of $(2.3 \pm 0.1) \times 10^3$ measured by Kirsch and Fuchs (1967). Since this shows better agreement with (1.6a) it may be that (1.6a) continues to improve as W decreases towards 2, but we still cannot account for the good agreement with (1.6b) at larger W. We may also comment that the weak variation of D with Re (*table V*) shows that Keller's formula is accurate to within 1% even for $Re = 5$ (at $W = 2.3$). This is one of the many examples of the success of lubrication theory outside the parameter range for which it is expected to hold.

Filter permeability k

This quantity is more useful than drag in studies of filter feeding. It was defined in eq. (1.3) as flow rate per unit force, or $U_0/\Delta\hat{p}$, and the dimensionless filter permeability is given by

$$\beta = \mu k/a = W/D. \tag{5.1}$$

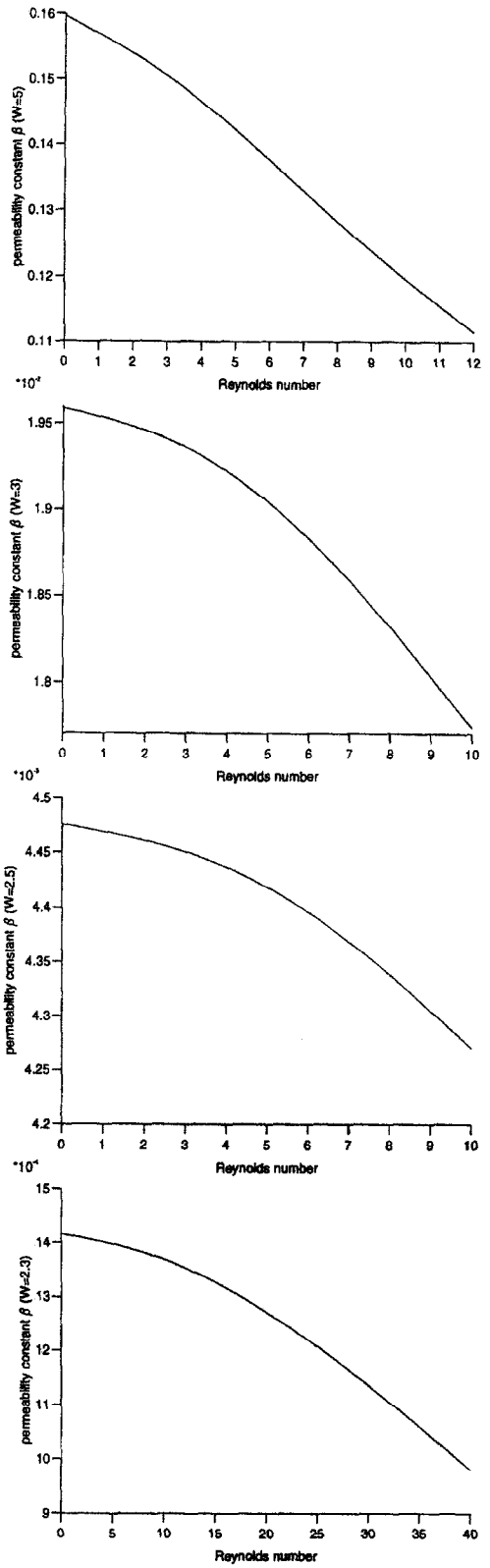

Fig. 10. – Filter permeability factor β plotted against Re for $W = 5, 3, 2.5, 2.3$.

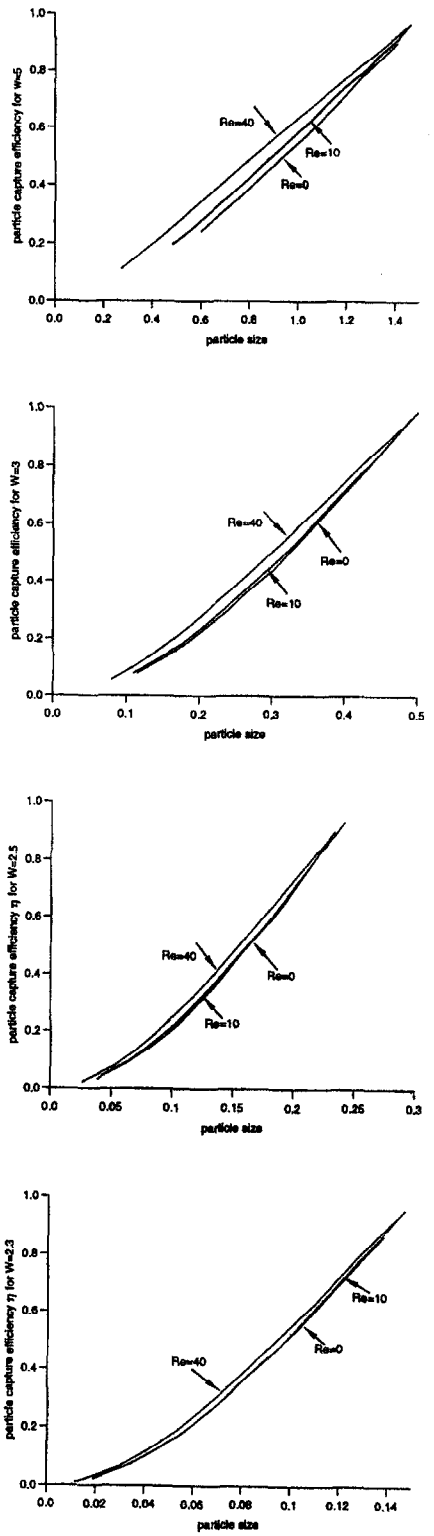

Fig. 11. – Particle capture efficiency η plotted against b for $Re = 0, 10, 40$ and $W = 5, 3, 2.5, 2.3$.

The quantity β is plotted against Re for four different cylinder spacings in *figures 10a-d* (note that the ordinates are scaled very differently). Clearly the (dimensionless) permeability decreases somewhat as Re increases, but decreases very rapidly as W decreases, as expected.

6. Particle interception and filter efficiency

As stated in the introduction we analyse the process of particle capture by direct interception. We assume that neutrally buoyant spherical particles of radius ba are uniformly (but sparsely) distributed in the oncoming flow. We also assume that the centre of any particle follows a streamline of the flow through the filter, as computed above, unless that streamline passes within a distance ba of a filter element, in which case the particle is deemed to be captured. These assumptions ignore the detailed final stages of the capture process, in which lubrication pressures will delay contact between particle and fibre, while electrostatic, van der Waals or other attractive forces may promote it, but will provide a useful guide to the capture efficiency of the filter.

We again consider just one "slice" of the (x, y) plane, between $y = 0$ and $y = W/2$, and let y_0 be the (dimensionless) y-coordinate far upstream ($x \to -\infty$) of a general streamline. We define $y_{0c}(b)$ as the value of y_0 for which the minimum distance between the streamline and the cylinder surface $x^2 + y^2 = 1$ is b. Thus if $y_0 > y_{0c}(b)$ the particle is not captured, while if $y_0 \leq y_{0c}(b)$ it is captured. Clearly, if $b \geq \frac{W}{2} - 1$, then $y_{0c}(b) = W/2$ and all particles are captured (sieving). The particle capture efficiency, or the proportion of oncoming particles (of radius b) that are captured, is

$$\eta(b) = \frac{2y_{0c}(b)}{W}, \tag{6.1}$$

which is equal to 1 when $b \geq W/2 - 1$. In general, η will depend on W and Re as well as on b.

It is easiest to calculate $y_{0c}(b)$ in an inverse way. That is, we choose a value of y_0, trace the streamline whose y coordinate tends to y_0 as $x \to -\infty$ ($\psi_0 = \frac{2y_0}{W}$), and record its distance of closest approach to the fibre: that is then the b for the given y_0. At zero Reynolds number, the point of closest approach is at $x = 0$, by symmetry; however, for non-zero Re it occurs at a value of $x < 0$. The computation of the points of closest approach requires very careful interpolation between the computed values of x, y and ψ at the grid points (i, j).

Figures 11(a-d) show particle capture efficiency η as a function of b (and Re) for $W = 5, 3, 2.5$ and 2.3 respectively. These figures reflect the fact that, in the present model, larger particles are captured by larger gaps between filter elements; they demonstrate also that increasing velocity (Re) has little effect on capture efficiency, especially when the gap between filter elements is reduced. For example, for $W = 2.3$ the particle capture efficiency of a filter element is almost unchanged as Re changes between 1 and 10. However, particle capture efficiency for a given b increases significantly as the spacing between two filter elements decreases. As an example, a particle with radius $b = 0.5$ is captured with efficiency of around 0.2 when the spacing is $W = 5$, but the capture efficiency for the same particle reaches 1 when the distance between two filtering elements is $W = 3$ (for $Re = 10$).

7. Conclusions

From the point of view of biologists studying filter feeding, the most important results from this paper are the predictions of filter permeability k and particle capture efficiency η. These are presented as functions of Reynolds number Re and (in the case of η) particle size b for several values of the fibre spacing W in *figures 10* and *11*. In the present case, of an infinite array of parallel fibres, it is clear that Re is a much less important

variable than W or b. This result should be contrasted with the predictions of Cheer and Koehl (1987) for a finite number (specifically, two) of parallel fibres, where the amount of flow going between the fibres depends strongly on Re as well as W.

It is of interest to apply our results to the two crustacean filters listed as examples in *table I*. On the third thoracic appendange of *D. parvula* the basic filter elements are the setules, for which $W = 4.2$ and $Re = 5 \times 10^{-5}$, which are sufficiently close to 5 and 0 respectively that we can use the formula of Tamada and Fujikawa (1957), ie: equations (1.4) and (1.5) to estimate the drag (see *table VI* for the accuracy at $W = 5$). This formula gives $D \approx 46.6$, so the dimensionless permeability = 0.09 (equation 5.1) and capture efficiency for $b = 1$ (particle diameter = setule diameter = 0.32 μm) will be around 0.6 or greater, estimated from *figure 11a* ($W = 5$). The corresponding results for the first maxilla of *E. pileatus* ($W = 6, Re = 0.1$) gives $D \approx 23.2, \beta = 0.26$ and $\eta(b = 1)$ around 0.5 or less. In dimensional terms, the two drag results correspond to filter pressure drops of $10Pa$ and $60Pa$ respectively, which give some indication of the strengths of these fine biological fibres.

The application of this work to biology can be fully worked out only after the "outer" problem has also been solved. That will require the calculation of flow through and around a finite sized filter with dimensionless permeability β as computed above. For a given distribution of food particle sizes this will also permit the solution of the optimisation problem outlined in the introduction: what is the optimal filter spacing for maximum food capture?

Acknowledgments. – This work was done while F.A. was a PhD student of T.J.P. in the Department of Applied Mathematical Studies at the University of Leeds. F.A. gratefully acknowledges the financial support of Balikesir University.

REFERENCES

BOHTE Z., 1975, Bounds for rounding errors in the Gaussian elimination for band systems, *J. Inst. Maths Applics.*, **16**, 133–142.

CHEER A. Y. L., KOEHL M. A. R., 1987, Paddles and rakes: fluid flow through bristled appendages of small organisms, *J. Theor. Biol.*, **129**, 17–39.

FORNBERG B., 1980, A numerical study of viscous flow past a circular cylinder, *J. Fluid Mech.*, **98**, 818–855.

FORNBERG B., 1985, Steady viscous flow past a circular cylinder up to Reynolds number 600, *J. Comput. Phys.*, **61**, 297–320.

FORNBERG B., 1988, Steady viscous flow past a sphere at high Reynolds numbers, *J. Fluid Mech.*, **190**, 471–489.

FORNBERG B., 1991, Steady incompressible flow past a row of circular cylinders, *J. Fluid Mech.*, **225**, 655–671.

FOX L., 1964, *An Introduction to numerical linear algebra*, Clarendon Press, Oxford, U.K.

GORDON D., 1978, Numerical calculations on viscous flow through cylinder arrays, *Comput. and Fluids*, **6**, 1–13.

HILDYARD M., 1987, *Fluid mechanics of the filter*, PhD Thesis, University of Leeds, U.K.

INGHAM D. B., TANG T., MORTON B. R., 1990, Steady two dimensional flow through a row of normal plates, *J. Fluid Mech.*, **210**, 281–302.

JØRGENSON C. B., 1966, *Biology of suspension feeding*, Pergamon, London, U.K.

JØRGENSON C. B., 1983, Fluid mechanical aspects of suspension feeding, *Mar. Ecol.-Prog. Ser.*, **11**, 89–103.

KELLER J. B., 1964, Viscous flow through a grating or lattice of cylinders, *J. Fluid Mech.*, **18**, 94–96.

KELLER H. B., TAKAMI H., 1966, Numerical studies of steady viscous flow about cylinders, *Numerical Solutions of Nonlinear Differential Equations*, ed. by D. Greenspan, John Wiley, New York, USA.

KIRSCH A. A., FUCHS N. A., 1967, The fluid flow in a system of parallel cylinders perpendicular to the flow direction at small Reynolds numbers, *J. Phys. Soc. Jpn*, **22**, 1251–1255.

LABARBERA M., 1984, Feeding currents and particle capture mechanisms in suspension feeding animals, *Am. Zool.*, **24**, 71–84.

LOUDON C., ALSTAD D. N., 1990, Theoretical mechanics of particle capture: predictions for hydropsychid caddisfly distributional ecology, *Am. Nat.*, **135**, 360–381.

MCLAUGHLIN C., MCCOMBER P., GAKWAYA A., 1986, Numerical calculation of particle collection by a row of cylinders in a viscous fluid, *Can. J. Chem. Eng.*, **64**, 205–210.

POWELL M. J. D., 1970, A hybrid method for nonlinear algebraic equations, in *Numerical Methods for Nonlinear Algebraic Equations*, ed. by Rabinowitz, P. Gordon and Breach, London, U.K., 87–114.

RUBENSTEIN D. I., KOEHL M. A. R., 1977, The mechanism of filter feeding: some theoretical considerations, *Amer. Nat.*, **111**, 981–994.

RUSSEL W. B., SAVILLE D. A., SCHOWALTER W. R., 1989, *Colloidal dispersions*, Cambridge University Press, U.K.

SILVESTER N. R., 1983, Some hydrodynamic aspects of filter feeding with rectangular-mesh nets, *J. Theor. Biol.*, **103**, 265–286.

TAMADA K., FUJIKAWA H., 1957, The steady two dimensional flow of a viscous fluid at low Reynolds numbers passing through an infinite row of equal parallel circular cylinders, *Q. J. Mech. Appl. Math.*, **10**, 423–431.

WILKINSON J. H., 1965, *The algebraic Eigenvalue Problem*, Clarendon Press, Oxford, U.K.

WILKINSON J. H., REINSCH C., 1971, *Handbook for Automatic Computation, Vol. II, Linear Algebra*, Springer, New York, USA.

(Received 2 October 1997;
revised 1 June 1998;
accepted 24 September 1998.)